Navier's slip condition and magnetic field effects on unsteady stagnation point flow subject to a stretched plate along to viscous dissipation and Joule heating utilizing nanofluids

Santosh Chaudhary[*] & K M Kanika

Department of Mathematics, Malaviya National Institute of Technology, Jaipur 302 017, India

This article mainly addresses Navier's slip boundary condition impact on two-dimensional, unsteady magneto hydrodynamic flow of electrically conducting viscous nanofluids adjacent to stagnation region due to a stretchable wall along to viscous dissipation and Joule heating. Nanofluids are taken namely silver-water, copper-water, titanium dioxide-water and alumina-water. Transformation procedure applied reduces the set of nonlinear partial differential equations into a system of nonlinear ordinary differential equations. Resulting governing boundary layer equations are numerically solved by establishing a Keller-box method. Effects of different nanofluids, stretching parameter, slip parameter; solid volume fraction, unsteadiness parameter, magnetic parameter and Eckert number on velocity and temperature distributions are illustrated via graphs and explained in details. Computational values of local skin friction and local Nusselt number for influences of specified parameters are found out and indicated in tabular mode. Moreover, dual solutions exist by cause of negative values of unsteadiness parameter in fluid flow, fluid temperature, wall shear stress and wall heat flux.

Keywords: Navier's slip condition, Magnetic field, Unsteady flow, Stagnation point, Stretched plate, Viscous dissipation, Joule heating, Nanofluids

1 Introduction

Boundary condition of Navier's slip enumerates the slip enclosed by the fluid tangential components and structure velocities is equivalent to fluid tangential component normal stress calculated near to the fluid-structure interface, whereas structure velocities and the fluid normal components are in continuous position. Needs of Navier's slip conditions have arisen for the demand of fluid-structure interaction issues associating structures of elastic along the rough boundaries and also towards a contact. These boundary conditions are integrated generally in the problems of fluid dynamics like macroscopic level. Applications of macroscopic have been examined extensively for both types of fluids Newtonian and non-Newtonian. Navier[1] developed the Navier's slip boundary condition and initiated that fluid flow component tangential to the wall would be equivalent towards the strain rate on wall. A literature survey of some comprehensive research about the fluid flow over the Navier's slip conditions is appeared by Chapouly[2], Nandeppanavar *et al.*[3], Ou and Ren[4], Seth and Mishra[5], and He *et al.*[6]

Magnetohydrodynamic (MHD) is the investigation of magnetic properties of electrically conducting fluids in which magnetic field induces current in the fluid. MHD model represents the combination of fluid equation and the electrodynamic Maxwell equations that receive the Lorentz force by the magnetic field. MHD flow has many applications in physics as well as engineering problems namely geophysics, in earth's core motion, MHD power generators design, solar physics, bearing, pumps and waste nuclear processing. For the first time, Pavlov[7] employed the theory of MHD flow due to a stretching wall. After that, Andersson[8] inspected the viscous fluid flow with magnetic field influence. Since then many researchers have spread out the idea of MHD flow for different fluid flow model like as Hujeirat[9], Robertsa and Kumar[10], Chaudhary and Kumar[11], Chaudhary and Choudhary[12] and Shit and Majee[13].

A fluid flow, whose properties such as density, velocity, pressure, etc., depend on the time, is called an unsteady flow. In common situations particularly flow in the heart, pulsating flow in arteries, flow over birds flapping wings and fish fins, appear an unsteady flow. Moreover, unsteady flow has importance in last several years for many applications like turbine

---

*Corresponding author (E-mail: d11.santosh@yahoo.com)

cascades in gas turbine engines and compressor blade areas. Stewartson[14] developed the theory of unsteady flow. On the other side, Gorla[15] and Hayat et al.[16] noted that theory and proposed the positions of flows during unsteady flow with various environments. For instance, some problems regarding to the unsteady flow can be found in the literature as Jat and Chaudhary[17], Nadeem and Saleem[18], and Chaudhary and Kumar[19].

Fluid motion near a stagnation region is known as stagnation point flow. This type of flow exists for all solid bodies, which are moving in a fluid. Entire kinetic energy is transformed into the internal energy at a stagnation point, so fluid velocity vanishes at that point. The greater heat transfer rate, pressure and mass deposition conflict at the stagnation region. Important applications of the stagnation point flow in the industrial processing are nuclear reactors cooling, glass blowing, electronic devices cooling through fan, metals continuous casting and melt-spinning processes. The analysis of two-dimensional flow nearby a stagnation region is initiated by Hiemenz[20] and got a similarity solution to the Navier-Stokes equations. Afterward, Chiam[21] continued this work by considering the stagnation point flow over stretching plate. Subsequently, King and Cox[22], Jat and Chaudhary[23], Mabood and Khan[24], Chaudhary and Choudhary[25], and Mahapatra and Sidui[26] discussed the behavior of fluid flow over a stagnation region under different situations.

Flow explorations past a stretching sheet have captivated the research community interest in behalf of their broad dimension of applications in the area of metallurgy and the polymer business. Relevant applications on these fields include construction of glass fiber, textiles and paper cooling, coating of wire and fiber, equipment of chemical processing, water and sewer pipes, and processing of food stuff. Initially, the pioneering concept of steady boundary layer flow of an incompressible fluid through a linearly stretched sheet is considered by Crane[27]. Following this work, Conti et al.[28] studied a numerical description of soft elastic apology of stretching plates of nematic elastomers. Several researchers such as Liao[29], Kelson[30], Chaudhary et al.[31], Weidman[32] and Liu and Liu[33] have presented the boundary layer flow towards a stretched surface along various stretching velocities like linear, quadratic, exponential, hyperbolic, oscillatory and radially.

Fluid viscosity produces resistance to motion, that in turn leads to conversion of mechanical energy to thermal energy. That type of procedure is known as viscous dissipation which acts such a source of energy. Whereas, Joule heating or ohmic heating occurs when conduction electrons collide with conductor's atom and release thermal energy. Viscous dissipation and Joule heating values have significant impact for heating and cooling of plate. There are a lot of applications in the area of industry and technology such as food processing, electric fuses, cartridge heaters, power generator systems, electronic cigarette and liquid metal fluids. El-Amin[34] inspected the first evaluation in this area and devoted the viscous dissipation and Joule heating effects. Moreover, convective flows of micropolar fluids by radiate isothermal porous mediums along to the influences of the viscous dissipation and Joule heating is analyzed by Rahman[35]. Recently, Chaudhary and Choudhary[36], and Mahanthesh and Gireesha[37] reported the explorations of fluid flow with the consideration of viscous dissipation and Joule heating condition.

The thermal conductivity of fluid is the most effectual aspect in heat transfer of fluid. Ordinary fluids have minor efficacy in heat transfer, so to expand the progress of fluid with high rate of heat transfer, a novel method as nanofluid has been devised. Nanofluid is the mixture of two elements such as solid nanoparticles and ordinary fluids. Sizes of nanoparticles are taken generally less than 100 nm by diameter and concentration of solids are held normally lower than 10 % beyond volume. Nanofluid has better thermal performance rather than base fluid, as proven by experiments. Thermal characteristics of nanofluid depend on the shape and size of particles, particle volume fraction, and material of particles, carrier fluid and temperature of fluid. Some appropriate applications of nanofluid are detergency, automotive, cancer therapy, high power lasers, oil engine transfer, lubrications, building cooling and heating, and heat exchanger equipments in the area of industry and manufacturing processes. Choi[38] is firstly coined the term nanofluid. Further, the illustration in a two-dimensional domain being increment of Buoyancy-driven heat transfer by applying nanofluids is presented by Khanafer et al.[39]. Later, fluid flow and heat transfer along to the different materials, shapes and size of nanoparticles are illustrated by numerous researchers like as Gumgum and Tezer-Sezgin[40], Mohammed and Narrein[41], Safikhani and Abbasi[42], and Aliabadian et al.[43]

Keeping the above literature survey in view, the ambition of current analysis is to continue the analysis of Malvandi et al.[44] by the impact of magnetic field on electrically conducting nanofluids in the appearance of viscous dissipation and Joule heating. To access the heat transfer rate and thermal conductivity of ordinary fluid, nanoparticles are exhausted such as silver (Ag), copper (Cu), titanium dioxide (TiO_2) and alumina (Al_2O_3) in the base fluid water.

2 Problem Developments

Consider an unsteady, laminar, two-dimensional boundary layer flow of water situated nanofluids involving four various types of solid nanoparticles like as Ag, Cu, TiO_2 and Al_2O_3 towards a stretching plate with free stream velocity $u_e = \dfrac{ax}{1 - ct}$ and surface velocity $u_w = \dfrac{bx}{1 - ct}$ respectively, where a, b and c are positive constants, x is the coordinate measured align to the stretched surface and t is the time. Cartesian coordinate system (x, y) is surmised in which $x-$ and $y-$directions are taken as the coordinates parallel to the plate and perpendicular to the plate, respectively. Figure 1 shows that plate is concurred by the plane $y = 0$ and fluid flow is confined in the upper half region $y \geq 0$. It is also suspected that surface temperature has a
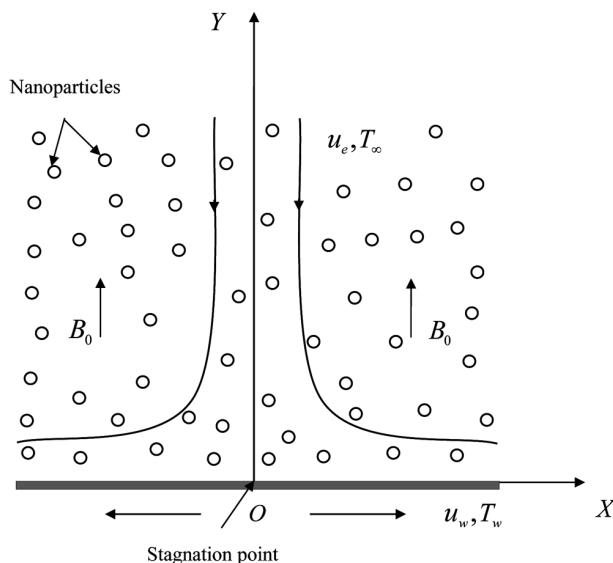

Fig. 1 – Physical geometry of the flow configuration.

constant value T_w and an ambient fluid temperature with constant value T_∞. Uniform magnetic field with strength B_0 is applied perpendicular to the plate and small value of the magnetic Reynolds number tends to negligible of an induced magnetic field. Further, to follow by Raza et al.[45], physical characteristics of base fluid and solid nanoparticles are exhibited in Table 1. By applying the mentioned considerations, the basic boundary layer equations are:

$$\frac{\partial u}{\partial x} + \frac{\partial v}{\partial y} = 0 \qquad \qquad \dots (1)$$

$$\frac{\partial u}{\partial t} + u \frac{\partial u}{\partial x} + v \frac{\partial u}{\partial y} = \frac{\partial u_e}{\partial t} + u_e \frac{du_e}{dx} + \upsilon_{nf} \left(\frac{\partial^2 u}{\partial x^2} + \frac{\partial^2 u}{\partial y^2} \right) - \frac{(\sigma_e)_{nf} B_0{}^2}{\rho_{nf}} (u - u_e)$$
$$\dots (2)$$

$$\frac{\partial T}{\partial t} + u \frac{\partial T}{\partial x} + v \frac{\partial T}{\partial y} = \alpha_{nf} \left(\frac{\partial^2 T}{\partial x^2} + \frac{\partial^2 T}{\partial y^2} \right) + \frac{\mu_{nf}}{(\rho C_p)_{nf}}$$

$$\left(\frac{\partial u}{\partial y} \right)^2 + \frac{(\sigma_e)_{nf} B_0{}^2}{(\rho C_p)_{nf}} (u - u_e)^2$$
$$\dots (3)$$

with the relevant boundary conditions

$$y = 0: \quad v = 0, \, u = u_w + u_{slip}, \, T = T_w$$
$$y \rightarrow \infty: \quad u \rightarrow u_e, \, T \rightarrow T_\infty \qquad \dots (4)$$

where, subscript nf indicates the nanofluid characteristics, u and v are the velocity factors corresponding to the $x-$ and $y-$axes, respectively, $\upsilon = \dfrac{\mu}{\rho}$ is the kinematic viscosity, μ is the coefficient of viscosity, ρ is the density, σ_e is the electrical conductivity, T is the temperature of nanofluid,

Table 1 – Physical characteristics of the fluid and the nanoparticles.

Materials	$\kappa (Wm^{-1}K^{-1})$	$\rho \, (Kgm^{-3})$	$C_p \, (JKg^{-1}K^{-1})$	$\sigma_e (Sm^{-1})$
Water	0.613	997.1	4179	0.05
Ag	429	10500	235	6.3×10^7
Cu	400	8933	385	5.96×10^7
TiO_2	8.9538	4250	686.2	0.24×10^7
Al_2O_3	40	3970	765	3.69×10^7

$\alpha = \dfrac{\kappa}{\rho C_p}$ is the thermal diffusivity, κ is the thermal conductivity, C_p is the specific heat at constant pressure, $u_{slip} = \upsilon N t^{1/2} \dfrac{\partial u}{\partial y}$ is the slip velocity and N is a slip factor constant. Consequently, second and third terms in right hand side of the energy Eq. (3) indicate the effect of viscous dissipation and Joule heating, respectively.

Moreover, pertinent physical properties of nanofluid restricted to spherical nanoparticles are coefficient of viscosity, density, electrical conductivity, thermal conductivity and heat capacitance proceed from Mohyud-Din *et al.*[46] are defined as follows:

$$\frac{\mu_{nf}}{\mu_f} = \frac{1}{\left(1 - \phi\right)^{5/2}} \qquad \dots (5)$$

$$\frac{\rho_{nf}}{\rho_f} = 1 - \phi + \phi \frac{\rho_s}{\rho_f} \qquad \dots (6)$$

$$\frac{(\sigma_e)_{nf}}{(\sigma_e)_f} = 1 + \frac{3\phi\left[\dfrac{(\sigma_e)_s}{(\sigma_e)_f} - 1\right]}{\dfrac{(\sigma_e)_s}{(\sigma_e)_f} + 2 - \phi\left[\dfrac{(\sigma_e)_s}{(\sigma_e)_f} - 1\right]} \qquad \dots (7)$$

$$\frac{\kappa_{nf}}{\kappa_f} = 1 + \frac{3\phi\left(\dfrac{\kappa_s}{\kappa_f} - 1\right)}{\dfrac{\kappa_s}{\kappa_f} + 2 - \phi\left(\dfrac{\kappa_s}{\kappa_f} - 1\right)} \qquad \dots (8)$$

$$\frac{(\rho C_p)_{nf}}{(\rho C_p)_f} = 1 - \phi + \phi \frac{(\rho C_p)_s}{(\rho C_p)_f} \qquad \dots (9)$$

where, subscripts f and s denote the physical properties for base fluid and nano sized solid particles, respectively and ϕ is the nanoparticle volume fraction.

3 Similarity Solution

By introducing the following similarity transformations (Malvandi *et al.*[44]):

$$\psi = \left(\frac{a\upsilon_f}{1 - ct}\right)^{1/2} x f(\eta), \quad \eta = \left[\frac{a}{\upsilon_f(1 - ct)}\right]^{1/2} y, \qquad \dots (10)$$

$$T = T_\infty + (T_w - T_\infty)\theta(\eta)$$

where, $\psi(x, y, t)$ is the stream function, which is defined in the regular manner as $u = \dfrac{\partial \psi}{\partial y}$ and $v = -\dfrac{\partial \psi}{\partial x}$, and likewise satisfy the continuity Eq. (1), $f(\eta)$ is the non-dimensional stream function, η is the similarity variable and $\theta(\eta)$ is the non-dimensional temperature.

Using the similarity variables Eq. (10), the momentum and the thermal energy Eqs (2) and (3) along to the boundary conditions Eq. (4) have been acquired as follows:

$$\frac{1}{\left(1 - \phi\right)^{5/2}\left(1 - \phi + \phi \dfrac{\rho_s}{\rho_f}\right)} f''' + \left(f - \frac{A}{2}\eta\right)f'' - (f' + A)f'$$
$$- \frac{1}{\left(1 - \phi + \phi \dfrac{\rho_s}{\rho_f}\right)} \frac{(\sigma_e)_{nf}}{(\sigma_e)_f} M(f' - 1) + A + 1 = 0 \qquad \dots (11)$$

$$\frac{\kappa_{nf}}{\kappa_f} \frac{1}{Pr} \theta'' + \left[1 - \phi + \phi \frac{(\rho C_p)_s}{(\rho C_p)_f}\right]\left(f - \frac{A}{2}\eta\right)\theta'$$
$$+ Ec\left[\frac{1}{\left(1 - \phi\right)^{5/2}} f''^2 + \frac{(\sigma_e)_{nf}}{(\sigma_e)_f} M(f' - 1)^2\right] = 0 \qquad \dots (12)$$

subject to the corresponding boundary conditions:

$$\eta = 0: \quad f = 0, \, f' = \varepsilon + \lambda f'', \, \theta = 1$$
$$\eta \to \infty: \quad f' \to 1, \, \theta \to 0 \qquad \dots (13)$$

where, prime (') expresses the differentiation with respect to η, $A = \dfrac{c}{a}$ is the unsteadiness parameter, $M = \dfrac{(\sigma_e)_f B_0^2 \upsilon_f Re_x}{\rho_f u_e^2}$ is the magnetic parameter, $Re_x = \dfrac{u_e x}{\upsilon_f}$ is the local Reynolds number, $Pr = \dfrac{\upsilon_f}{\alpha_f}$

is the Prandtl number, $Ec = \dfrac{u_e^{\,2}}{(C_p)_f (T_w - T_\infty)}$ is the Eckert number, $\varepsilon = \dfrac{b}{a}$ is the stretching parameter and $\lambda = \upsilon N \left[\dfrac{at}{\upsilon_f (1 - ct)} \right]^{1/2}$ is the slip parameter.

4 Important Physical Parameters

Quantities of practical interest are the local skin friction coefficient C_f and the local Nusselt number Nu_x, which are declared in the dimensional form as:

$$C_f = \frac{\tau_w}{\dfrac{\rho_f u_e^{\,2}}{2}}, \quad Nu_x = \frac{x q_w}{\kappa_f (T_w - T_\infty)} \qquad \dots (14)$$

where,

$$\tau_w = \mu_{nf} \left(\frac{\partial u}{\partial y} \right)_{y=0} \quad \text{and} \quad q_w = -\kappa_{nf} \left(\frac{\partial T}{\partial y} \right)_{y=0} \quad \text{are the}$$

wall shear stress and the wall heat flux, respectively.

By employing the dimensionless variables Eq. (10), the physical quantities Eq. (14) can be expressed as:

$$\mathrm{Re}_x^{1/2} C_f = \frac{2}{(1-\phi)^{5/2}} f''(0), \quad \frac{1}{\mathrm{Re}_x^{1/2}} Nu_x = -\frac{\kappa_{nf}}{\kappa_f} \theta'(0) \quad \dots (15)$$

5 Numerical Procedures

Keller box method is applied to determine the computational solution of the governing ordinary differential Eqs (11) and (12) with the appropriate boundary conditions Eq. (13). Convenient finite value towards the far field boundary condition $\eta \to \infty = 4$ is surmised for the numerical solution.

5. 1 Implicit finite difference scheme

Introducing new dependent variables:

$$f' = p \qquad \dots (16)$$
$$p' = q \qquad \dots (17)$$
$$\theta' = s \qquad \dots (18)$$

Thus, the Eqs (11) and (12) can be written as:

$$\frac{1}{(1-\phi)^{5/2} \left(1 - \phi + \phi \dfrac{\rho_s}{\rho_f} \right)} q' + \left(f - \frac{A}{2} \eta \right) q - (p + A)p$$
$$- \frac{1}{\left(1 - \phi + \phi \dfrac{\rho_s}{\rho_f} \right)} \frac{(\sigma_e)_{nf}}{(\sigma_e)_f} M(p - 1) + A + 1 = 0 \qquad \dots (19)$$

$$\frac{\kappa_{nf}}{\kappa_f} \frac{1}{\mathrm{Pr}} s' + \left[1 - \phi + \phi \frac{(\rho C_p)_s}{(\rho C_p)_f} \right] \left(f - \frac{A}{2} \eta \right) s +$$
$$Ec \left[\frac{1}{(1-\phi)^{5/2}} q^2 + \frac{(\sigma_e)_{nf}}{(\sigma_e)_f} M(p-1)^2 \right] = 0 \qquad \dots (20)$$

with the associated boundary conditions Eq. (13) becomes:

$$\eta = 0: \quad f = 0, \; p = \varepsilon + \lambda q, \; \theta = 1$$
$$\eta \to \infty: \quad p \to 1, \; \theta \to 0 \qquad \dots (21)$$

Figure 2 represents the rectangular grid $X\eta -$ plane and the net points delineated as follows:

$$x_0 = 0, \; x_i = x_{i-1} + k_i, \; i = 1,2,3,....I$$
$$\eta_0 = 0, \; \eta_j = \eta_{j-1} + h_j, \; j = 1,2,3,....J \qquad \dots (22)$$

Finite difference form of the Eqs (16) to (20) for the midpoint $\left(x_i, \eta_{j-\frac{1}{2}} \right)$ of the segment QR by using centered difference derivatives are given as:

$$f_j - f_{j-1} - \frac{h_j}{2}(p_j + p_{j-1}) = 0 \qquad \dots (23)$$

$$p_j - p_{j-1} - \frac{h_j}{2}(q_j + q_{j-1}) = 0 \qquad \dots (24)$$

$$\theta_j - \theta_{j-1} - \frac{h_j}{2}(s_j + s_{j-1}) = 0 \qquad \dots (25)$$
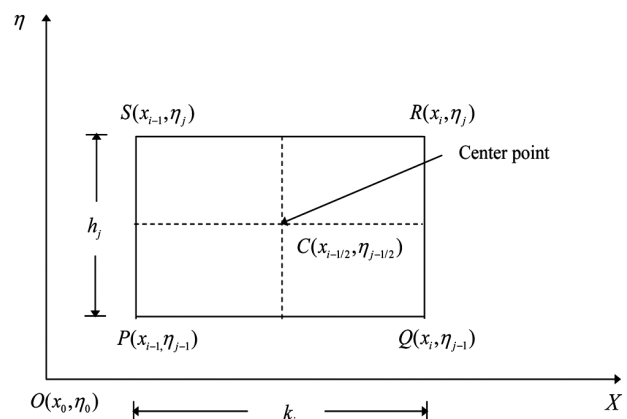

Fig. 2 – Net rectangle for finite difference grid point.

$$\frac{1}{h_j(1-\phi)^{5/2}\left(1-\phi+\phi\frac{\rho_s}{\rho_f}\right)}(q_j - q_{j-1})$$

$$+\frac{1}{4}\big[(f_j + f_{j-1}) - A\eta\big](q_j + q_{j-1}) - \frac{1}{4}\big[(p_j + p_{j-1}) + 2A\big](p_j + p_{j-1})$$

$$-\frac{1}{2\left(1-\phi+\phi\frac{\rho_s}{\rho_f}\right)}\frac{(\sigma_e)_{nf}}{(\sigma_e)_f}M\big[(p_j + p_{j-1}) - 2\big] + A + 1 = 0$$

$$\dots (26)$$

$$\frac{1}{h_j}\frac{\kappa_{nf}}{\kappa_f}\frac{1}{\mathrm{Pr}}(s_j - s_{j-1}) + \frac{1}{4}\left[1-\phi+\phi\frac{(\rho C_p)_s}{(\rho C_p)_f}\right]\big[(f_j + f_{j-1}) - A\eta\big](s_j + s_{j-1})$$

$$+\frac{1}{4}Ec\left\{\frac{1}{(1-\phi)^{5/2}}(q_j + q_{j-1})^2 + \frac{(\sigma_e)_{nf}}{(\sigma_e)_f}M\big[(p_j + p_{j-1}) - 2\big]^2\right\} = 0$$

$$\dots (27)$$

Equations (23) to (27) are established for $j = 1, 2, 3, \dots J-1$ and from the associated boundary conditions Eq. (21), at initial condition $j = 0$ and far field condition $j = J$ it is noted that:

$$f_0 = 0, \quad p_0 = \varepsilon + \lambda q_0, \quad \theta_0 = 1, \quad p_J \to 1, \quad \theta_J \to 0$$
$$\dots (28)$$

5.2 Method of Newton

To linearize the nonlinear structure, Newton's method is used. Following iterations are introduced:

$$f_j^{(i+1)} = f_j^{(i)} + \delta f_j^{(i)}, \ p_j^{(i+1)} = p_j^{(i)} + \delta p_j^{(i)}, \ q_j^{(i+1)} = q_j^{(i)} + \delta q_j^{(i)},$$

$$\theta_j^{(i+1)} = \theta_j^{(i)} + \delta \theta_j^{(i)}, \ s_j^{(i+1)} = s_j^{(i)} + \delta s_j^{(i)}$$
$$\dots (29)$$

Substituting the above expression into the Eqs (23) to (27) and then decline quadratic and higher order terms in $\delta f_j^{(i)}$, $\delta p_j^{(i)}$, $\delta q_j^{(i)}$, $\delta\theta_j^{(i)}$ and $\delta s_j^{(i)}$. Thus above scheme yields a tridiagonal structure as:

$$\delta f_j - \delta f_{j-1} - \frac{h_j}{2}(\delta p_j + \delta p_{j-1}) = (r_1)_{j-\frac{1}{2}} \quad \dots (30)$$

$$\delta p_j - \delta p_{j-1} - \frac{h_j}{2}(\delta q_j + \delta q_{j-1}) = (r_2)_{j-\frac{1}{2}} \quad \dots (31)$$

$$\delta \theta_j - \delta \theta_{j-1} - \frac{h_j}{2}(\delta s_j + \delta s_{j-1}) = (r_3)_{j-\frac{1}{2}} \quad \dots (32)$$

$$(a_1)_{j-\frac{1}{2}}\delta f_j + (a_2)_{j-\frac{1}{2}}\delta f_{j-1} + (a_3)_{j-\frac{1}{2}}\delta p_j + (a_4)_{j-\frac{1}{2}}\delta p_{j-1}$$
$$+ (a_5)_{j-\frac{1}{2}}\delta q_j + (a_6)_{j-\frac{1}{2}}\delta q_{j-1} = (r_4)_{j-\frac{1}{2}} \quad \dots (33)$$

$$(b_1)_{j-\frac{1}{2}}\delta f_j + (b_2)_{j-\frac{1}{2}}\delta f_{j-1} + (b_3)_{j-\frac{1}{2}}\delta p_j$$
$$+ (b_4)_{j-\frac{1}{2}}\delta p_{j-1} + (b_5)_{j-\frac{1}{2}}\delta q_j + (b_6)_{j-\frac{1}{2}}\delta q_{j-1} + (b_7)_{j-\frac{1}{2}}\delta s_j \dots$$
$$+ (b_8)_{j-\frac{1}{2}}\delta s_{j-1} = (r_5)_{j-\frac{1}{2}}$$
$$\dots (34)$$

where,

$$(a_1)_{j-\frac{1}{2}} = (a_2)_{j-\frac{1}{2}} = \frac{1}{4}(q_j + q_{j-1}),$$

$$(a_3)_{j-\frac{1}{2}} = (a_4)_{j-\frac{1}{2}} = -\frac{1}{4}(p_j + p_{j-1}) - \frac{1}{2\left(1-\phi+\phi\frac{\rho_s}{\rho_f}\right)}\frac{(\sigma_e)_{nf}}{(\sigma_e)_f}M - \frac{A}{2},$$

$$(a_5)_{j-\frac{1}{2}} = \frac{1}{h_j(1-\phi)^{5/2}\left(1-\phi+\phi\frac{\rho_s}{\rho_f}\right)} + \frac{1}{4}(f_j + f_{j-1}) - \frac{A}{4}\eta,$$

$$(a_6)_{j-\frac{1}{2}} = -\frac{1}{h_j(1-\phi)^{5/2}\left(1-\phi+\phi\frac{\rho_s}{\rho_f}\right)} + \frac{1}{4}(f_j + f_{j-1}) - \frac{A}{4}\eta,$$

$$(b_1)_{j-\frac{1}{2}} = (b_2)_{j-\frac{1}{2}} = \frac{1}{4}\left[1-\phi+\phi\frac{(\rho C_p)_s}{(\rho C_p)_f}\right](s_j + s_{j-1}),$$

$$(b_3)_{j-\frac{1}{2}} = (b_4)_{j-\frac{1}{2}} = \frac{1}{4}\frac{(\sigma_e)_{nf}}{(\sigma_e)_f}M\,Ec\big[(p_j + p_{j-1}) - 4\big],$$

$$(b_5)_{j-\frac{1}{2}} = (b_6)_{j-\frac{1}{2}} = \frac{1}{4(1-\phi)^{5/2}}Ec(q_j + q_{j-1}),$$

$$(b_7)_{j-\frac{1}{2}} = \frac{1}{h_j}\frac{\kappa_{nf}}{\kappa_f}\frac{1}{\mathrm{Pr}} + \frac{1}{4}\left[1-\phi+\phi\frac{(\rho C_p)_s}{(\rho C_p)_f}\right]\big[(f_j + f_{j-1}) - A\eta\big],$$

$$(b_8)_{j-\frac{1}{2}} = -\frac{1}{h_j}\frac{\kappa_{nf}}{\kappa_f}\frac{1}{\mathrm{Pr}} + \frac{1}{4}\left[1-\phi+\phi\frac{(\rho C_p)_s}{(\rho C_p)_f}\right]\big[(f_j + f_{j-1}) - A\eta\big],$$

$$(r_1)_{j-\frac{1}{2}} = -(f_j - f_{j-1}) + \frac{h_j}{2}(p_j + p_{j-1}),$$

$$(r_2)_{j-\frac{1}{2}} = -(p_j - p_{j-1}) + \frac{h_j}{2}(q_j + q_{j-1}),$$

$$(r_3)_{j-\frac{1}{2}} = -(\theta_j - \theta_{j-1}) + \frac{h_j}{2}(s_j + s_{j-1}),$$

$$(r_4)_{j-\frac{1}{2}} = -\frac{1}{h_j(1-\phi)^{5/2}\left(1-\phi+\phi\frac{\rho_s}{\rho_f}\right)}(q_j - q_{j-1})$$

$$-\frac{1}{4}\left[(f_j + f_{j-1}) - A\eta\right](q_j + q_{j-1}) + \frac{1}{4}\left[(p_j + p_{j-1}) + 2A\right](p_j + p_{j-1})$$

$$+\frac{1}{2\left(1-\phi+\phi\frac{\rho_s}{\rho_f}\right)}\frac{(\sigma_e)_{nf}}{(\sigma_e)_f}M\left[(p_j + p_{j-1}) - 2\right]$$

and

$$(r_5)_{j-\frac{1}{2}} = -\frac{1}{h_j}\frac{\kappa_{nf}}{\kappa_f}\frac{1}{\text{Pr}}(s_j - s_{j-1}) - \frac{1}{4}\left[1-\phi+\phi\frac{(\rho C_p)_s}{(\rho C_p)_f}\right]\left[(f_j + f_{j-1}) - A\eta\right](s_j + s_{j-1})$$

$$-\frac{1}{4}Ec\left\{\frac{1}{(1-\phi)^{5/2}}(q_j + q_{j-1})^2 + \frac{(\sigma_e)_{nf}}{(\sigma_e)_f}M\left[(p_j + p_{j-1}) - 2\right]^2\right\}.$$

For all iterates, it is considered as:

$$\delta f_0 = 0, \quad \delta p_0 = 0, \quad \delta\theta_0 = 0, \quad \delta p_J = 0, \quad \delta\theta_J = 0 \quad \dots (35)$$

5.3 Block elimination method

Writing Eqs (30) to (34) in the form of block tridiagonal matrix:

$$\begin{bmatrix} [A_1] & [C_1] & & & \\ [B_2] & [A_2] & [C_2] & & \\ & \ddots & \ddots & \dots & \\ & & [B_{J-1}] & [A_{J-1}] & [C_{J-1}] \\ & & & [B_J] & [A_J] \end{bmatrix} \begin{bmatrix} [\delta_1] \\ [\delta_2] \\ \vdots \\ [\delta_{J-1}] \\ [\delta_J] \end{bmatrix} = \begin{bmatrix} [r_1] \\ [r_2] \\ \vdots \\ [r_{J-1}] \\ [r_J] \end{bmatrix}$$

that is

$$[A][\delta] = [r] \qquad \dots (36)$$

where, the elements are

$$[A_1] = \begin{bmatrix} 0 & 0 & 1 & 0 & 0 \\ \dfrac{-h_j}{2} & 0 & 0 & \dfrac{-h_j}{2} & 0 \\ 0 & \dfrac{-h_j}{2} & 0 & 0 & \dfrac{-h_j}{2} \\ a_6 & 0 & a_1 & a_5 & 0 \\ b_6 & b_8 & b_1 & b_5 & b_7 \end{bmatrix},$$

$$[A_j] = \begin{bmatrix} \dfrac{-h_j}{2} & 0 & 1 & 0 & 0 \\ -1 & 0 & 0 & \dfrac{-h_j}{2} & 0 \\ 0 & -1 & 0 & 0 & \dfrac{-h_j}{2} \\ a_4 & 0 & a_1 & a_5 & 0 \\ b_4 & 0 & b_1 & b_5 & b_7 \end{bmatrix} \quad \text{for } 2 \le j \le J,$$

$$[B_j] = \begin{bmatrix} 0 & 0 & -1 & 0 & 0 \\ 0 & 0 & 0 & \dfrac{-h_j}{2} & 0 \\ 0 & 0 & 0 & 0 & \dfrac{-h_j}{2} \\ 0 & 0 & a_2 & a_6 & 0 \\ 0 & 0 & b_2 & b_6 & b_8 \end{bmatrix} \quad \text{for } 2 \le j \le J,$$

$$[C_j] = \begin{bmatrix} \dfrac{-h_j}{2} & 0 & 0 & 0 & 0 \\ 1 & 0 & 0 & 0 & 0 \\ 0 & 1 & 0 & 0 & 0 \\ a_3 & 0 & 0 & 0 & 0 \\ b_3 & 0 & 0 & 0 & 0 \end{bmatrix} \quad \text{for } 1 \le j \le J-1,$$

$$[\delta_1] = \begin{bmatrix} \delta q_0 \\ \delta s_0 \\ \delta f_1 \\ \delta q_1 \\ \delta s_1 \end{bmatrix}, \quad [\delta_j] = \begin{bmatrix} \delta p_{j-1} \\ \delta\theta_{j-1} \\ \delta f_j \\ \delta q_j \\ \delta s_j \end{bmatrix} \quad \text{for } 2 \le j \le J$$

and $[r_j] = \begin{bmatrix} (r_1)_j \\ (r_2)_j \\ (r_3)_j \\ (r_4)_j \\ (r_5)_j \end{bmatrix}$ for $1 \le j \le J$.

Forward sweep: To solve the Eq. (36), matrix A is assumed as a nonsingular matrix then matrix A can be written as:

$$[A] = [L][U] \qquad \dots (37)$$

with

$$[L] = \begin{bmatrix} [\alpha_1] & & & & \\ [B_2] & [\alpha_2] & & & \\ & & \ddots & & \\ & & & [\alpha_{J-1}] & \\ & & & [B_J] & [\alpha_J] \end{bmatrix} \quad \text{and}$$

$$[U] = \begin{bmatrix} I & [\beta_1] & & & \\ & I & [\beta_2] & & \\ & & \ddots & \ddots & \\ & & & I & [\beta_{J-1}] \\ & & & & I \end{bmatrix}$$

where, I is the identity matrix of order 5×5, and $[\alpha_j]$ and $[\beta_j]$ are the matrix of order 5×5, whose elements are driven by the following relations:

$$[\alpha_1] = [A_1] \qquad \dots (38)$$

$$[A_1][\beta_1] = [C_1] \qquad \dots (39)$$

$$[\alpha_j] = [A_j] - [B_j][\beta_{j-1}],$$
$$j = 2, 3, \dots J \qquad \dots (40)$$

Backward sweep:
In view of:

$$[L][U][\delta_j] = [r_j] \qquad \dots (41)$$

with the consideration as:

$$[U][\delta_j] = [W_j] \qquad \dots (42)$$

$$[L][W_j] = [r_j] \qquad \dots (43)$$

where, $[W_j]$ are the column matrix of order 5×1 and elements of $[W_j]$ can be found out from Eq. (43) as:

$$[\alpha_1][W_1] = [r_1] \qquad \dots (44)$$

$$[\alpha_j][W_j] = [r_j] - [B_j][W_{j-1}], \quad 2 \le j \le J \qquad \dots (45)$$

A track in which $[\alpha_j]$, $[\beta_j]$ and $[W_j]$ are described in commonly point out to as the forward sweep. While once the elements of $[W_j]$ are predicted, the Eq. (42) disposes the solution known as backward sweep, whose elements can be obtained by the given relations:

$$[\delta_j] = [W_j] - [\beta_j][\delta_{j+1}], \quad 1 \le j \le J - 1 \qquad \dots (46)$$

$$[\delta_J] = [W_J] \qquad \dots (47)$$

These iteration process are replicated up till convergence rule is fulfilled with maintaining an accuracy of 10^{-7} and process are stopped when, $\left| \delta q_0^{(i)} \right| \le \xi$, where ξ is a small prescribed value.

6 Validation of Proposed Method

Computational values of $f''(0)$ and $\theta'(0)$ achieved by the Keller box scheme are compared with the earlier published research Malvandi et al.[44] for the correctness of computed values. These comparisons are shown quantitatively in Table 2, which confirms the accuracy of the current results and validate the proposed method.

7 Results and Discussion

In this section, graphical discussion of the computational results of the velocity $f'(\eta)$ and the temperature $\theta(\eta)$ profiles are represented for the distinct types of nanofluids and certain changes in dimensionless parameters such as the stretching parameter ε, the slip parameter λ, the solid volume fraction ϕ, the unsteadiness parameter A, the magnetic parameter M and the Eckert number Ec along to the Cu − water nanofluid. Influence of different nanoparticles with base fluid water as well as considering parameters on the surface shear stress $f''(0)$ and the surface heat flux $\theta'(0)$ are also

Table 2 – Comparison for the numerical values of $f''(0)$ and $\theta'(0)$ with previously published data when $\varepsilon = \lambda = M = 0.0$, $Pr = 6.2$ and $Ec = 0.0$.

Nanofluids	ϕ	A	$f''(0)$		$-\theta'(0)$	
			Malvandi et al.[44]	Present results	Malvandi et al.[44]	Present results
Cu − water	0.1	1	1.76039	1.760599	0.46870	0.4693227
	0.2		1.82528	1.825489	0.46779	0.4683050
TiO_2 − water	0.1		1.51280	1.513035	0.40757	0.4091370
	0.2		1.45746	1.457736	0.39199	0.3947570
	0.1	-1	0.93199	0.931840	1.50207	1.4902520
			-0.99451	-1.014180	0.45293	0.4240258
	0.2		0.89790	0.897760	1.35558	1.3257900
			-0.95813	-0.987400	0.41189	0.3755330
Al_2O_3 − water	0.1	1	1.49669	1.496943	0.40320	0.4050094
	0.2		1.43248	1.432778	0.38477	0.3883884

illustrated through tables. Moreover due to finding out the impact of anyone pertinent parameter on velocity profile, temperature profile, surface shear stress and heat transfer rate, all remaining specified parameters are taken as constant.

Figures 3 and 4 demonstrate the impacts of various nanofluids namely Ag – water, Cu – water, TiO_2 – water and Al_2O_3 – water on the fluid flow $f'(\eta)$ and the fluid temperature $\theta(\eta)$, respectively. It can be seen from these figures that the fluid velocity decreases with the serial of nanofluids like Ag – water, Cu – water, TiO_2 – water and Al_2O_3 – water, while reverse is happened in the temperature of fluid along to the same sequence of nanofluids. This is due to the reason that with the change of nanoparticles adjacent in base fluid water, the fluid flow and the fluid temperature change because distinct types of nanoparticles have various mechanical and physical characteristics namely density, coefficients of thermal expansion and dynamic viscosity.

Influences of the stretching parameter ε on the velocity $f'(\eta)$ and the temperature $\theta(\eta)$ distributions

are mentioned in Figs 5 and 6, respectively. These figures found that an enhancement in the values of the stretching parameter ε leads to an enlargement in the momentum boundary layer, even though the thermal boundary layer have opposite effect. This is consequence of the fact that stretching parameter is the ratio of the stretching velocity to the free stream velocity. Stretching velocity controls the free stream velocity and also rises rapidly than free stream velocity as stretching parameter rises. So fluid velocity enhances and fluid temperature declines.

Figures 7 and 8 show the changes in the dimensionless velocity $f'(\eta)$ and the dimensionless temperature $\theta(\eta)$, with respect to several values of the slip parameter λ, respectively. It is clear from these figures that along to the raises in the value of slip parameter λ, the velocity step-up and the temperature step-down. Because over to the slip condition, extraction in stretching plate is partially communicated within the fluid and heat transfer from heated surface into the adjacent fluid is in few quantities.
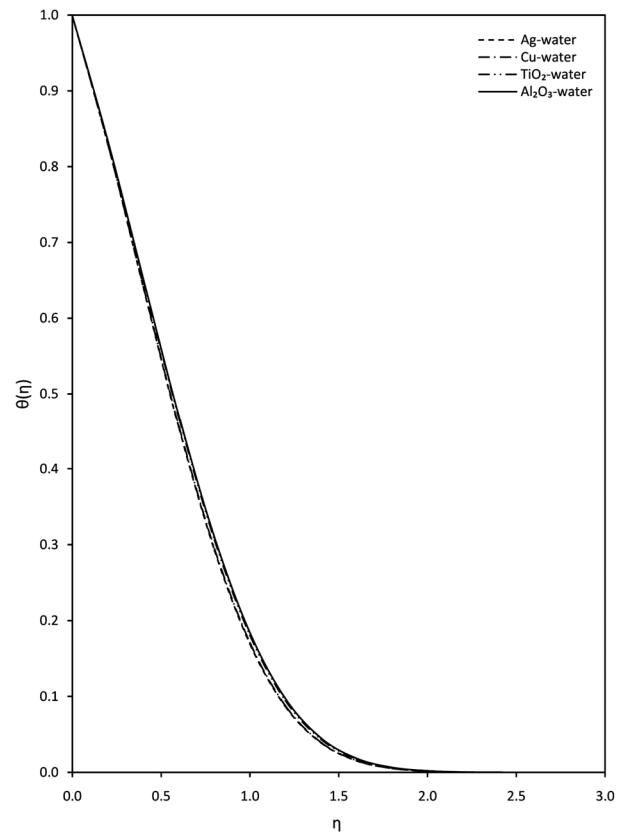

Fig. 3 – Velocity profiles versus η for different types of nanofluids when $\varepsilon = 0.1$, $\lambda = 0.1$, $\phi = 0.04$, $A = 0.5$ and $M = 0.1$.

Fig. 4 – Temperature profiles versus η for different types of nanofluids when $\varepsilon = 0.1$, $\lambda = 0.1$, $\phi = 0.04$, $A = 0.5$, $M = 0.1$, $Pr = 6.2$ and $Ec = 0.1$.
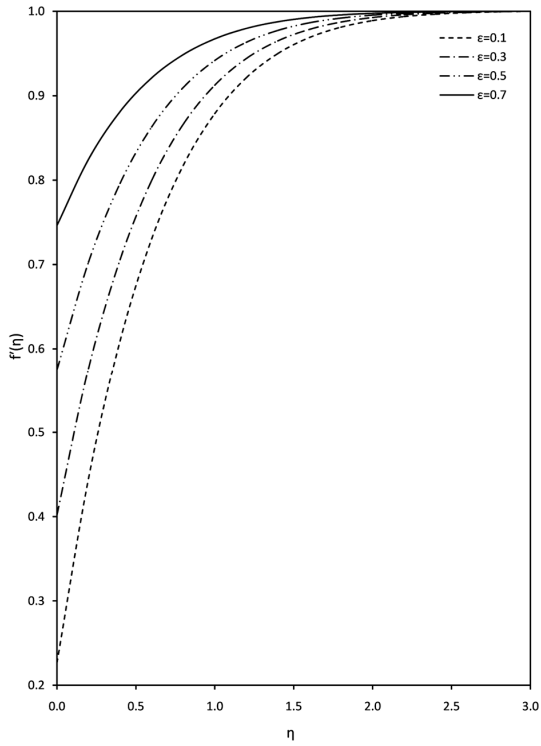
Fig. 5 – Velocity profiles of Cu – water nanofluid versus η for different values of ε when $\lambda = 0.1$, $\phi = 0.04$, $A = 0.5$ and $M = 0.1$.
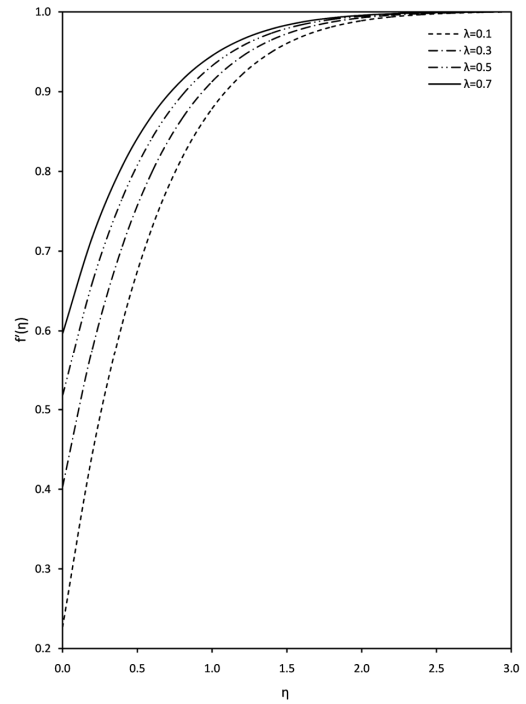

Fig. 7 – Velocity profiles of Cu – water nanofluid versus η for different values of λ when $\varepsilon = 0.1$, $\phi = 0.04$, $A = 0.5$ and $M = 0.1$.
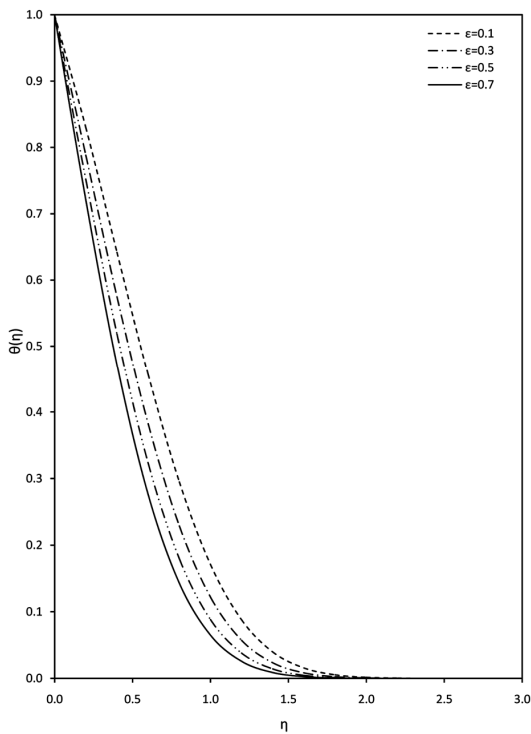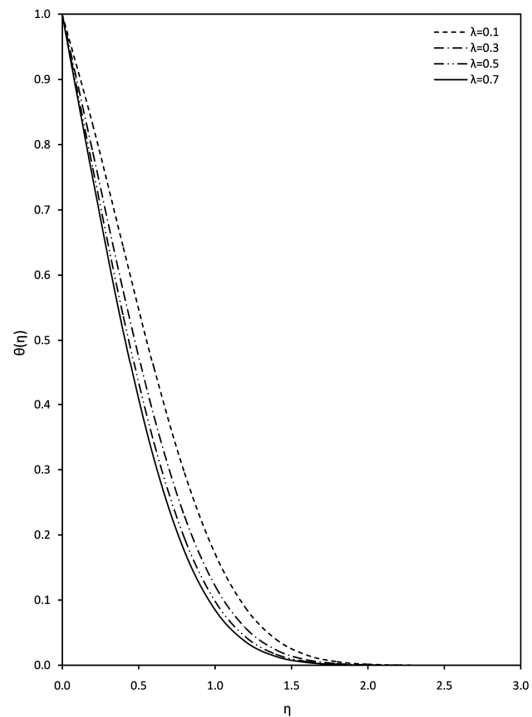

Fig. 6 – Temperature profiles of Cu – water nanofluid versus η for different values of ε when $\lambda = 0.1$, $\phi = 0.04$, $A = 0.5$, $M = 0.1$, $\Pr = 6.2$ and $Ec = 0.1$.

Fig. 8 – Temperature profiles of Cu – water nanofluid versus η for different values of λ when $\varepsilon = 0.1$, $\phi = 0.04$, $A = 0.5$, $M = 0.1$, $\Pr = 6.2$ and $Ec = 0.1$.

Variations of the velocity $f'(\eta)$ and the temperature $\theta(\eta)$ profiles for the impacts of the solid volume fraction ϕ are presented through Figs 9 and 10, respectively. From these figures, it may be observed that the momentum boundary layer as well as the thermal boundary layer develop for the increment in the value of the solid volume fraction ϕ. From a physical aspect, solid nanoparticles have cumulative resistance of flow, which accelerates the fluid flow. Further, thermal conductivity of nanofluid evolves with the enlargement in solid volume fraction, that in turn increases the temperature field.

Figures 11 to 12 and 13 to 14 depict the effects of the unsteadiness parameter A on the flow of fluid $f'(\eta)$ and the temperature of fluid $\theta(\eta)$, respectively. It is found from Figs 11 and 13 that the fluid flow and the temperature increase over the booming value of the unsteadiness parameter A,

while reverse is true in velocity when $\eta > 1.5$. Subsequently, dual solutions exist for negative values of the unsteadiness parameter A, which are illustrated in Figs 12 and 14. It is delightful to detected via these figures that by the enhancement in the unsteadiness parameter A there is accretion in the dimensionless velocity and the dimensionless temperature for both first and second solution branches, although reversal impact can be seen in fluid velocity for first solution when $\eta > 1.4$ and for second solution when $\eta > 0.4$. It is also interesting to note in second solution branch that the velocity distribution reduces in installment for the range of $0.4 < \eta < 0.9$. This can attribute to the reason that wall declines heat along to the enhancement in the unsteadiness parameter, which leads depreciates in temperature, but due to the stagnation region, the temperature of fluid grows-up.
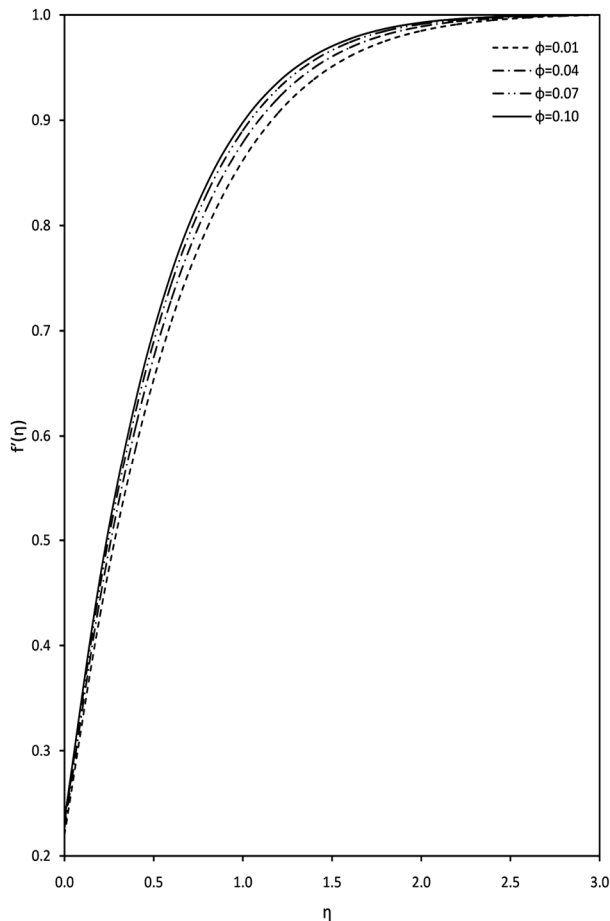

Fig. 9 – Velocity profiles of $Cu-$ water nanofluid versus η for different values of ϕ when $\varepsilon = 0.1$, $\lambda = 0.1$, $A = 0.5$ and $M = 0.1$.
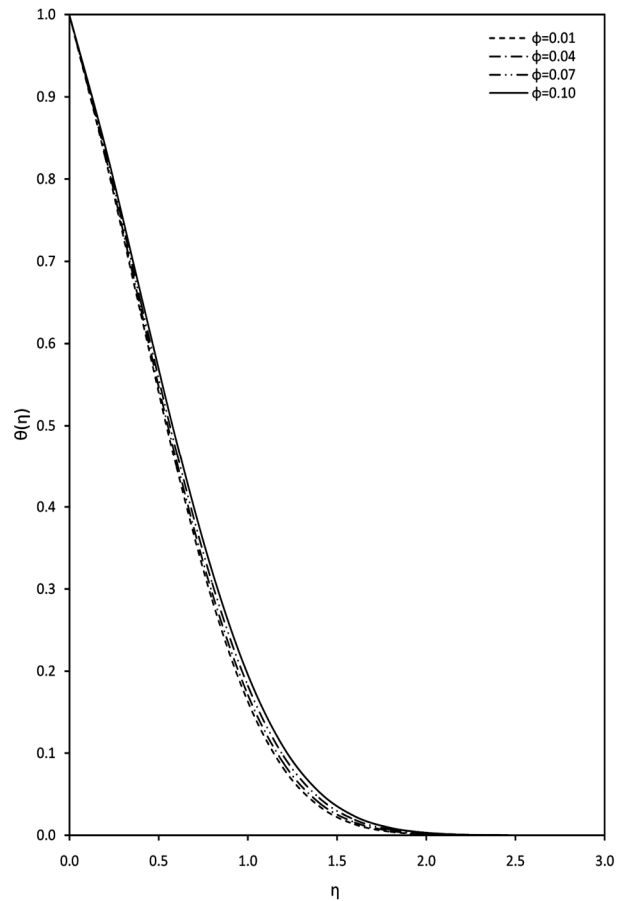

Fig. 10 – Temperature profiles of $Cu-$ water nanofluid versus η for different values of ϕ when $\varepsilon = 0.1$, $\lambda = 0.1$, $A = 0.5$, $M = 0.1$, $\mathrm{Pr} = 6.2$ and $Ec = 0.1$.

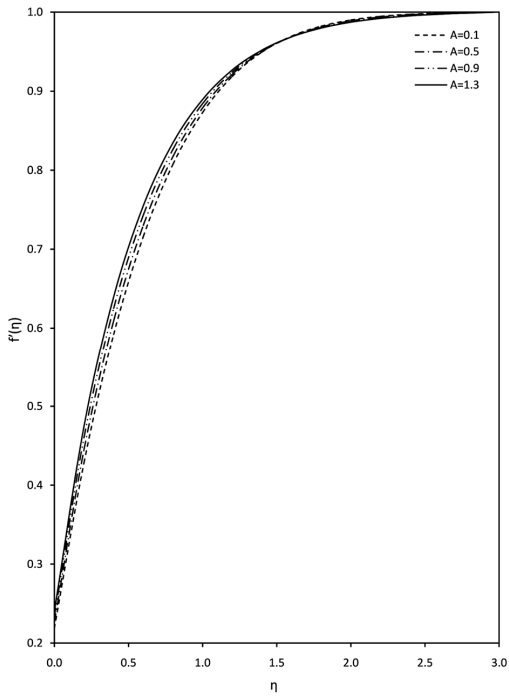Fig. 11 – Velocity profiles of Cu – water nanofluid versus η for different values of A when $\varepsilon = 0.1$, $\lambda = 0.1$, $\phi = 0.04$ and $M = 0.1$.

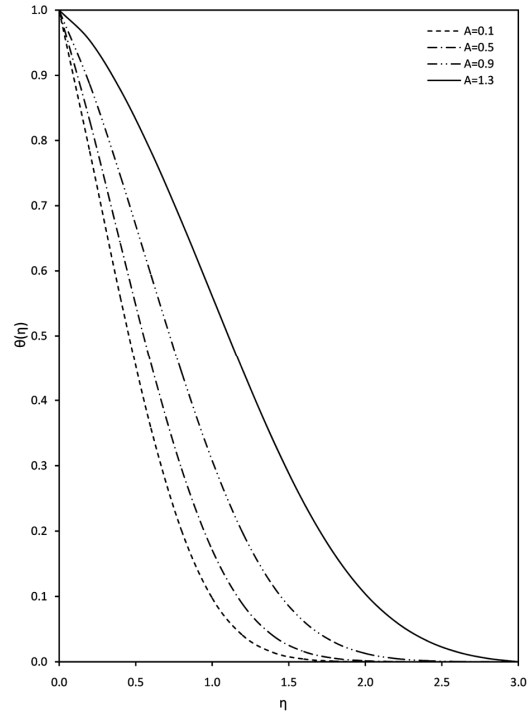Fig. 13 – Temperature profiles of Cu – water nanofluid versus η for different values of A when $\varepsilon = 0.1$, $\lambda = 0.1$, $\phi = 0.04$, $M = 0.1$, Pr $= 6.2$ and $Ec = 0.1$.
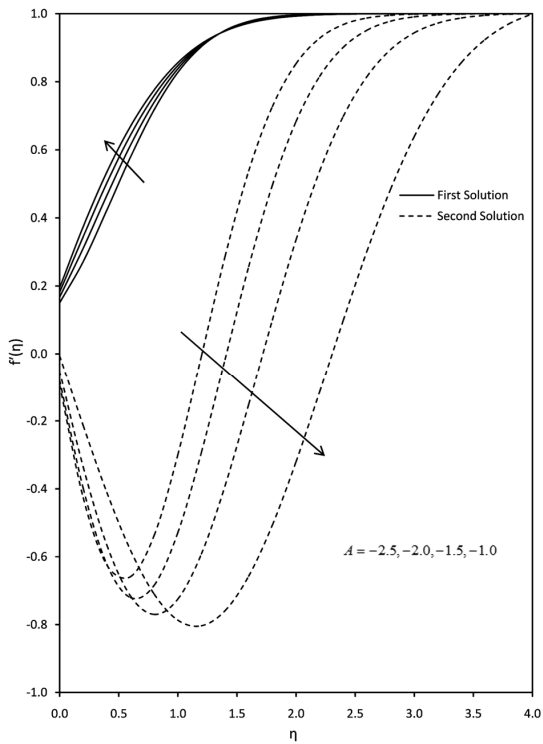

Fig. 12 – Velocity profiles of Cu – water nanofluid versus η for different values of A when $\varepsilon = 0.1$, $\lambda = 0.1$, $\phi = 0.04$ and $M = 0.1$
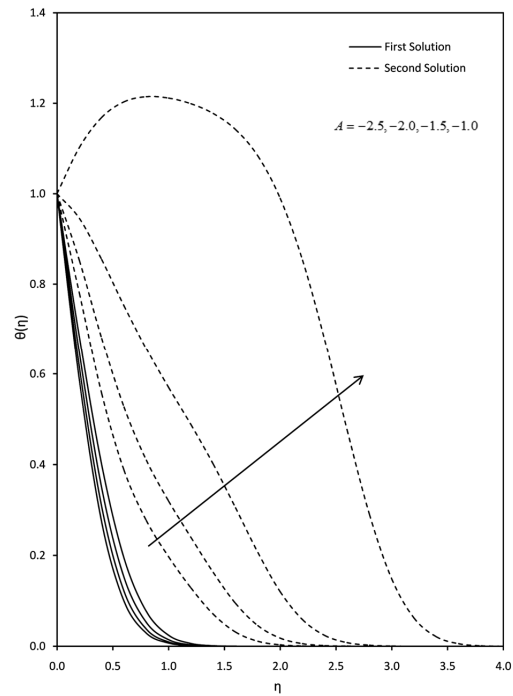

Fig. 14 – Temperature profiles of Cu – water nanofluid versus η for different values of A when $\varepsilon = 0.1$, $\lambda = 0.1$, $\phi = 0.04$, $M = 0.1$, Pr $= 6.2$ and $Ec = 0.1$.

Profiles of the velocity $f'(\eta)$ and the temperature $\theta(\eta)$ for the influence of the magnetic parameter M are plotted in the Figs. 15 and 16, respectively. These figures show that enhancing value of the magnetic parameter M implies that the fluid velocity is the increasing function, while reverse behavior is found in the temperature field. Physically, it occurs because the larger value of the magnetic parameter yields a drag type force as Lorentz force, that type of force leads to the resistive improvement into the fluid motion and creates more heat resulting in an increment of the fluid temperature.

Figure 17 indicates reflect of the Eckert number Ec on the temperature $\theta(\eta)$ distribution. This figure displays that accretion in the Eckert number Ec implies to enlargement in the thermal boundary layer thickness. This is because Eckert number is proportional to the flow kinetic energy and inversely proportional to the difference of boundary layer enthalpy. Viscous dissipation influence on the
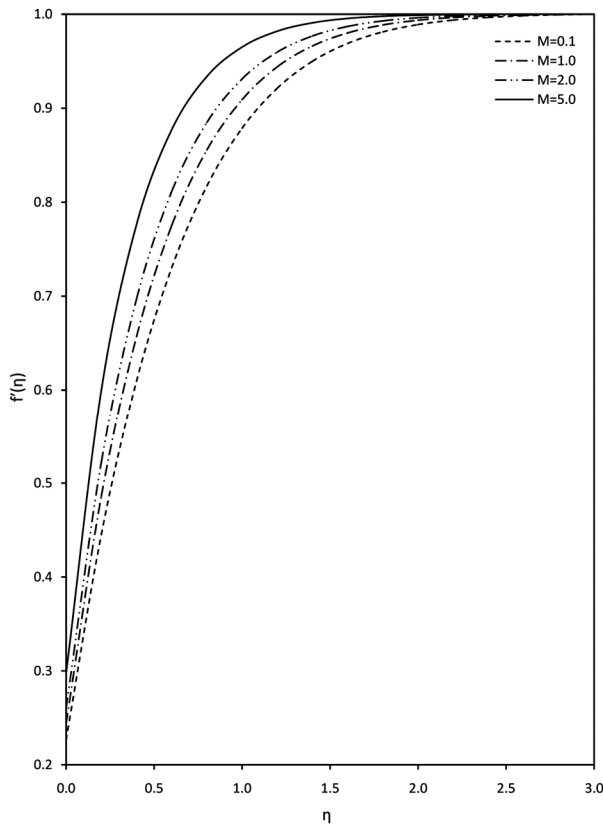

Fig. 16 – Temperature profiles of $Cu-$water nanofluid versus η for different values of M when $\varepsilon = 0.1$, $\lambda = 0.1$, $\phi = 0.04$, $A = 0.5$, $\mathrm{Pr} = 6.2$ and $Ec = 0.1$.

Fig. 15 – Velocity profiles of $Cu-$water nanofluid versus η for different values of M when $\varepsilon = 0.1$, $\lambda = 0.1$, $\phi = 0.04$ and $A = 0.5$.
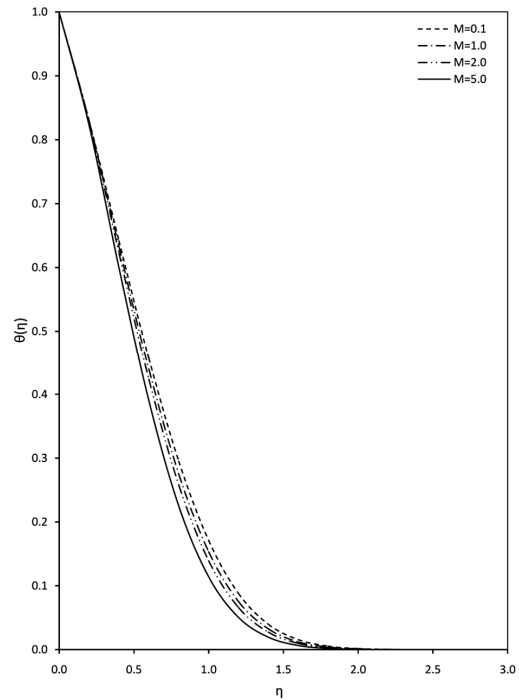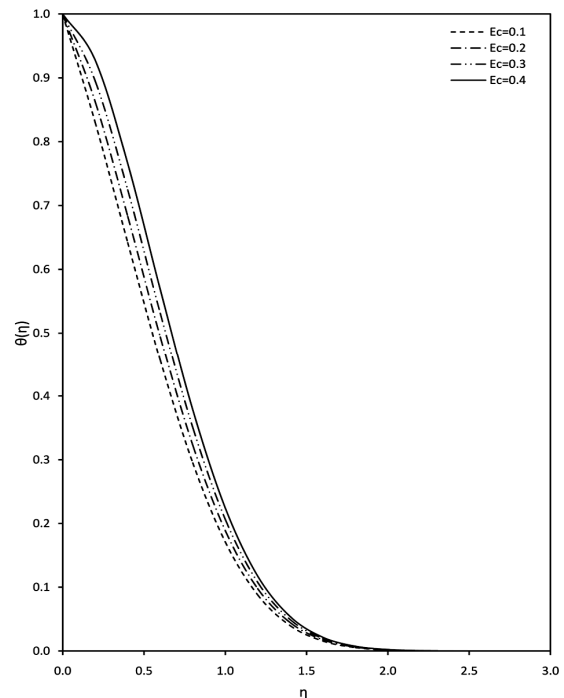

Fig. 17 – Temperature profiles of $Cu-$water nanofluid versus η for different values of Ec when $\varepsilon = 0.1$, $\lambda = 0.1$, $\phi = 0.04$, $A = 0.5$, $M = 0.1$ and $\mathrm{Pr} = 6.2$.

fluid velocity leads to the increment in energy, which accommodating a high temperature of fluid and also higher buoyancy force. An enhancement in the buoyancy force along to the dissipation parameter increment tends to the step-up in fluid temperature.

Implementation of the four different types of nanofluids and controlling parameters like as the stretching parameter ε, the slip parameter λ, the solid volume fraction ϕ, the unsteadiness parameter A, the magnetic parameter M and the Eckert number Ec on the surface shear stress $f''(0)$ and the surface heat flux $\theta'(0)$ are given in Table 3. Further by the Eq. (15), the wall shear stress $f''(0)$ and the heat transfer rate $\theta'(0)$ are proportional to the local skin friction C_f and the local Nusselt number Nu_x respectively. According to this table, the wall shear stress $f''(0)$ declines along with increasing order of the nanofluids particularly Ag – water, Cu – water, TiO_2 – water and Al_2O_3 –

water, although the rate of heat transfer $\theta'(0)$ step-up with the growing up manner of nanofluids such as Cu – water, Ag – water, TiO_2 – water and Al_2O_3 – water. Consequently, it is apparent that the local skin friction C_f and the local Nusselt number Nu_x reduce with the rising value of the stretching parameter ε and the slip parameters λ, however opposite phenomenon creates for some raise in the value of the solid volume fraction ϕ, the unsteadiness parameter A and the magnetic parameter M. It is also revealed that the rate of heat transfer $\theta'(0)$ increases by development in the Eckert number Ec. From the practical viewpoint, negative values of the heat flux lead to the statement that there is a heat flow to the plate.

Dual solutions of the surface shear stress $f''(0)$ and the surface heat flux $\theta'(0)$ for various values of the unsteadiness parameter A are delineated in Table 4. This table characterizes that for first solution and second solution branches, shear stress as well as heat transfer rate step-up due to the rising values of the unsteadiness parameter A.

Table 3 – Computational values of $f''(0)$ and $\theta'(0)$ for different types of nanofluids and several values of the relevant physical parameters when $Pr = 6.2$.

Nanofluids	ε	λ	ϕ	A	M	Ec	$f''(0)$	$-\theta'(0)$
Ag – water	0.1	0.1	0.04	0.5	0.1	0.1	1.277140	0.762957
Cu – water							1.252158	0.763390
TiO_2 – water							1.173015	0.752902
Al_2O_3 – water							1.168047	0.750239
Cu – water	0.3						1.007327	1.008073
	0.5						0.741953	1.222008
	0.7						0.457880	1.404274
	0.1	0.3					1.005836	1.009412
		0.5					0.832838	1.153975
		0.7					0.707842	1.246249
		0.1	0.01				1.188244	0.787819
			0.07				1.299380	0.734897
			0.10				1.333217	0.703908
			0.04	0.1			1.176500	1.013159
				0.9			1.322786	0.473630
				1.3			1.388960	0.131217
				0.5	1.0		1.426047	0.721931
					2.0		1.586363	0.685334
					5.0		1.951718	0.607871
					0.1	0.2	1.252158	0.517270
						0.3		0.271150
						0.4		0.025030

Table 4 – Dual solutions of $f''(0)$ and $\theta'(0)$ in $Cu-$water nanofluid with several values of A when $\varepsilon = 0.1$, $\lambda = 0.1$, $\phi = 0.04$, $M = 0.1$, $Pr = 6.2$ and $Ec = 0.1$.

A	$f''(0)$		$-\theta'(0)$	
	First solution	Second solution	First solution	Second solution
-2.5	0.49620	-1.91850	2.147863	0.9415770
-2.0	0.66240	-1.77090	1.973326	0.5798980
-1.5	0.80760	-1.50660	1.781543	0.1400570
-1.0	0.93642	-1.04512	1.570395	-0.5927513

8 Conclusions

Study of a numerical problem with viscous dissipation and Joule heating influence on an unsteady boundary layer flow of several types of electrically conducting nanofluids near a stagnation region due to the stretched wall with Navier's slip boundary condition in the magnetic field is established. Governing partial differential equations are reduced into the nonlinear ordinary differential equations by utilizing the convenient similarity transformations. Keller box method is applied to the computational solution of the resulting differential equations. Following main findings are extracted from this problem:

(i) $Ag-$water has higher fluid flow and local skin friction, while Al_2O_3-water has lower fluid flow and local skin friction as compared to the remaining nanofluids namely $Cu-$water and TiO_2-water. Whereas, Al_2O_3-water nanofluid has better improvement on the fluid temperature as well as the rate of heat transfer than other nanofluids,

(ii)   Increasing nature of the stretching parameter, the slip parameter, the solid volume fraction, the unsteadiness parameter and the magnetic parameter lead to enhancement in the momentum boundary layer, the thermal boundary layer, the surface shear stress and the surface heat flux. Until opposite behavior is noted in the fluid velocity when $\eta > 1.5$ for the unsteadiness parameter and also the dimensionless temperature, the wall shear stress and the rate of heat transfer have reverse phenomenon for rising values of the stretching parameter and the slip parameter. Even though the fluid temperature declines for the step-up in the magnetic parameter,

(iii)   Dual solution branches for the reaction of access negative values of the unsteadiness parameter is directed towards to cause the development in the fluid flow, the fluid temperature, the local skin friction and the local Nusselt number, whereas fluid flow reduces when $\eta > 1.4$ in first solution branch and also decreases when $\eta > 0.4$ in second solution branch. It is also concluded for second solution branch that velocity profile diminishes partially within the range of η from 0.4 to 0.9,

(iv)   The temperature field as well as the local Nusselt number rise along to the booming value of the Eckert number.

References

1   Navier C L M H, *Memoires de l'Academic Royale des Sciences de l'nstitut de France*, 6 (1823) 389.
2   Chapouly M, *J Differ Equations*, 247 (2009) 2094.
3   Nandeppanavar M M, Vajravelu K, Abel M S & Siddalingappa M N, *Int J Therm Sci*, 58 (2012) 143.
4   Ou Y & Ren D, *J Math Anal Appl*, 420 (2014) 1316.
5   Seth G S & Mishra M K, *Adv Powder Technol*, 28 (2017) 375.
6   He Q, Glowinski R & Wang X P, *J Comput Phys*, 366 (2018) 281.
7   Pavlov K B, *Magnetohydrodynamic*, 10 (1974) 507.
8   Andersson H I, *Acta Mech*, 95 (1992) 227.
9   Hujeirat A, *Comput Phys Commun*, 168 (2005) 1.
10   Robertsa S A & Kumar S, *Phys Fluids*, 22 (2010) 122102.
11   Chaudhary S & Kumar P, *Meccanica*, 49 (2014) 69.
12   Chaudhary S & Choudhary M K, *Eng Comput*, 35 (2018) 1675.
13   Shit G C & Majee S, *Int J Heat Fluid Flow*, 70 (2018) 237.
14   Stewartson K, *Adv Appl Mech*, 6 (1960) 1.
15   Gorla R S R, *Fluid Dynamics Res*, 15 (1995) 237.
16   Hayat T, Asghar S & Siddiqui A M, *Int J Eng Sci*, 38 (2000) 337.
17   Jat R N & Chaudhary S, *Il Nuovo Cimento*, 124 B (2009) 53.
18   Nadeem S & Saleem S, *J Taiwan Inst Chem E*, 44 (2013) 596.
19   Chaudhary S & Kumar P, *J Appl Math Phys*, 3 (2015) 921.
20   Hiemenz K, *Dingler's Polytech J*, 326 (1911) 321.
21   Chiam T C, *J Phys Soc Jpn*, 63 (1994) 2443.
22   King J R & Cox S M, *Stud Appl Math*, 115 (2005) 73.
23   Jat R N & Chaudhary S, *Z Angew Math Phys*, 61 (2010) 1151.
24   Mabood F & Khan W A, *Comput Fluids*, 100 (2014) 72.
25   Chaudhary S & Choudhary M K, *Indian J Pure Appl Phys*, 54 (2016) 209.
26   Mahapatra T R & Sidui S, *Euro J Mech- B/Fluids*, 65 (2017) 522.
27   Crane L J, *J Appl Math Phys*, 21 (1970) 645.
28   Conti S, Desimone A & Dolzmann G, *J Mech Phys Solids*, 50 (2002) 1431.
29   Liao S J, *Stud Appl Math*, 117 (2006) 2529.
30   Kelson N A, *Int J Non-Linear Mech*, 46 (2011) 1090.
31   Chaudhary S, Choudhary M K & Sharma R, *Meccanica*, 50 (2015) 1977.
32   Weidman P, *Int J Non-Linear Mech*, 82 (2015) 1.
33   Liu L & Liu F, *Appl Math Lett*, 79 (2018) 92.
34   El-Amin M F, *J Magn Magn Mater*, 263 (2003) 337.
35   Rahman M M, *Commun Nonlinear Sci Numer Simul*, 14 (2009) 3018.

36 Chaudhary S & Choudhary M K, *Indian J Pure Appl Phys*, 55 (2017) 864.
37 Mahanthesh B & Gireesha B J, *Res Phys*, 8 (2018) 869.
38 Choi S U S, *Publ Fed*, 231 (1995) 99.
39 Khanafer K, Vafai K & Lightstone M, *Int J Heat Mass Transf*, 46 (2003) 3639.
40 Gumgum S & Tezer-Sezgin M, *Eng Anal Bound Elem*, 34 (2010) 727.
41 Mohammed H A & Narrein K, *Int Commun Heat Mass Transf*, 39 (2012) 1375.
42 Safikhani H & Abbasi F, *Adv Powder Technol*, 26 (2015) 1609.
43 Aliabadian E, Kamkar M, Chen Z & Sundararaja U, *Phys Fluids*, 31 (2019) 013104.
44 Malvandi A, Hedayati F & Ganji D D, *Powder Technol*, 253 (2014) 377.
45 Raza J, Rohni A M & Omar Z, *Math Comput Appl*, 21 (2016) doi:10.3390/mca21040043.
46 Mohyud-Din S T, Khan U & Hassan S M, *Adv Mech Eng*, 8 (2016) 1.